

A Simulator of Atom-Atom Entanglement with Atomic Ensembles and Quantum Optics

Ruilin Zhou

Xuanying Lai

Yuhang Gan

University of California, Santa Cruz

University of Texas at Dallas

University of California, Santa Cruz

Katia Obraczka

Shengwang Du

Chen Qian

University of California, Santa Cruz

University of Texas at Dallas

University of California, Santa Cruz

Abstract—One fundamental goal of quantum networks is to provide node-to-node entanglement distribution. In this work, we develop a simulator, called A²Tango, for entanglement generation between two remote atom-ensemble nodes in a quantum network following Briegel, Dur, Cirac and Zoller (BDCZ) protocol. We encode quantum information to the two spatial modes of local atomic-ensemble spin waves and polarization states of single photons. The basic operations include atom-photon entanglement generation, quantum memory write-read operations, two-photon Bell-state measurement, and quantum state tomography. We model multi-photon events during the local excitation and propagation to account for their induced error in entanglement generation and distribution. We investigate the entanglement generation rate and fidelity as functions of the parameters which are realizable in experiments. Our work improves the open-sourced SeQUENCe simulator and inspires the development of future quantum networks.

Index Terms—quantum networks, entanglement, simulator

I. INTRODUCTION

The rapid development of quantum technologies has resulted in a growing interest in quantum networks, which aim to facilitate communication and computation using quantum mechanical properties. One of the key objectives of a quantum network is to establish node-to-node entanglements, a fundamental building block for many information-processing tasks in quantum networks with high memory efficiency. We argue that no existing quantum simulator simulates the Briegel, Dur, Cirac and Zoller (BDCZ) protocol [1], a potential building block for quantum networks with high memory efficiency, which generates entanglement between two atomic ensembles. In this work, in order to fill this fundamental gap, we develop a quantum simulator called A²Tango that models the BDCZ protocol. Our contributions are as follows:

- A²Tango extends the open-source Simulator of QUantum Network Communication(SeQUENCe) to model atomic node entanglements according to the BDCZ protocol. We add modules that model atomic node ensembles and Bell-State measurement (BSM). **We plan to make our simulator open-source once our paper is accepted for publication.**
- To simulate BSM, we model the process of atom-photon entanglement as a *creation* operator and the detection of the photon as an *annihilation* operator.
- A²Tango simulates the BDCZ protocol to generate entanglement between two atomic ensembles. Specifically,

we simulate the error induced by multiple atom-photon events. We study the entanglement success probability and fidelity. The tomography of two photons to reconstruct the original density matrix is also modeled.

The rest of the paper is organized as follows: In Section II, we briefly introduce different physical systems used in quantum networks, the general procedure to generate entanglement between different nodes we use in A²Tango, and current quantum network simulators. In Section III, we describe A²Tango in detail, namely how it models cold atomic ensembles and their corresponding basic operations including atom-photon entanglement, atom-atom entanglement, bell state measurement, and quantum tomography. We also describe how we model multiple photon events. In Section IV, we discuss how A²Tango implements the models. Section V presents preliminary simulation results.

II. BACKGROUND AND RELATED WORK

A. Entanglement Generation Using Different Physical Systems

Quantum network nodes can be realized with different physical systems to generate node-node entanglement. Here we briefly summarize some well-studied and promising schemes. For a more detailed and comprehensive survey on different platforms, we refer the reader to [2]

- Single neutral atoms: Single atoms placed in optical cavities enhance light-matter interaction strength and have been extensively studied over the past two decades. They exhibit remarkable properties for quantum information processing with high fidelity and long coherence time and robust light-matter interfaces.
- Trapped ions: Trapped ions provide longer storage time compared to neutral atoms, can be near-deterministically detected through optical cycling transitions, and offer high-fidelity implementation of single-ion operations and quantum memory.
- Nitrogen-Vacancy (NV) centers in diamond: NV centers, which are point defects in the diamond lattice, have been widely used in quantum information processing due to their compatibility with existing technology.
- Cold atomic ensembles: Previous schemes based on single atom/ion/defect have small cross sections to interact with single photons, which result in very low quantum

memory efficiencies ($< 10\%$) and limit their applications. This matter-photon interaction can be significantly improved by the collective enhancement of million atoms. Cold atomic ensembles have been demonstrated as the most efficient ($> 85\%$) quantum memories [3] for single-photon qubits and have promising features for distributed quantum computing [4]. Our simulator simulates cold atomic ensemble quantum nodes.

B. Entanglement Generation with Atomic Ensembles

One fundamental goal of a quantum network is to deliver entangled pairs between non-adjacent nodes. The first step is to generate entanglement between two adjacent nodes. In our simulator and experiments, we follow three steps to model entanglement between non-adjacent nodes: First, we implement two atom-photon entanglements separately on two adjacent nodes. Second, we send the entangled flying photons to an intermediate station, a BSM node, and perform Bell State Measurement. Eventually, we verify the entanglement between two atomic ensembles. We followed the well-known solutions [5], [6] and experimental setup [7] which combines the DLCZ [8] protocol and the strategy in BDCZ [9]. The main advantage of this approach compared to previous ones is that it no longer requires long-distance phase stability which is 7 orders of magnitude looser than in the DLCZ protocol [5]. Another advantage is that, after a few entanglement connections, the vacuum component can be suppressed and no longer dominates. In terms of generating atom-photon entanglement, different from previous work realized with trapped ions [10], a single atom in a cavity [11] and two spatially separated atomic ensembles [12], the method in our work adopts two collective excitations in different spatial modes of a single atomic ensemble to implement the atom-photon entanglement. Cold atomic ensembles have been demonstrated as the most efficient quantum memories [3] for single-photon qubits due to their collective enhancement and have promising features for distributed quantum computing [4]. A major disadvantage of such a scheme is the low entanglement swapping rate due to the postselection based on BSM two-photon coincidence. Such limitation could be compensated by its up to sub-second long quantum memory lifetime [13].

C. Quantum Network Simulator

A^2Tango goes beyond current quantum network simulators. More specifically, it extends the Simulator of QUantum Network Communication (SeQUENCe) [14] which is a customizable, modularized, discrete event simulator for quantum networks, which simulates the hardware all the way to the control plane. The two most important modules of SeQUENCe are Simulation Kernels which manage the discrete event simulation functionality and quantum state and the Hardware components which are used to model different real hardware devices. In terms of experimental hardware, SeQUENCe focuses on the simulation of single rare-earth ion memories and provides different encoding types of quantum

states such as time-bin, polarization, and single-atom. Similarly to SeQUENCe, NetSquid [15] also aims at simulating physical devices and uses a modular design that is not tied to a particular network stack. NetSquid provides some optimization on the kernel which enables the scalability of up to 1000 nodes and faster computation. Unlike SeQUENCe, NetSquid focuses on the simulation of NV centers, atomic frequency combs, and electronically induced transparency. Aiming to model the physical layer of the quantum network and to provide a specific representation of quantum states, SimulQron [16] is a quantum network simulator designed to facilitate the development and testing of quantum network applications and protocols and with a specific focus on simulating the application layer of the quantum network. QuNetSim [17] focuses on the simulation of upper-level quantum network protocols and does not focus on a specific physical model; SQUANCH [18] provides agent-based modeling and provides a configurable error model at the physical layer, but it does not have a discrete event simulator kernel and thus cannot keep track of time which is crucial in quantum network research, e.g., when studying generate rate and time-dependent noise which impact the coherence of the quantum state; QuISP [19] is another open-source quantum network simulator that, like the previous two simulators, places emphasis on scalability. However, it distinguishes itself by tracking the error models of qubits rather than their quantum state representations, such as density matrices or key vectors. This approach allows for efficient simulations of large-scale quantum networks while still providing insights into the effects of errors on system performance.

III. MODELS FOR SIMULATIONS

Unlike SeQUENCe, which employs the spontaneous parametric down-conversion (SPDC) photon source model, A^2Tango models a cold atomic ensemble to generate atom-photon entanglements, which inherently serves as quantum memory with high efficiency and long coherence time. With photonic polarization BSM acting as entanglement swapping, we can create atom-atom entanglement from two pairs of atom-photon entanglement. More practically, we model polarization BSM as well as state tomography with multiphoton-induced error, which provides insight into experimental design and optimization.

A. Atom-Photon Entanglement Generated by Cold Atomic Ensembles

In A^2Tango , each quantum node is equipped with a laser-cooled ^{87}Rb atomic ensemble trapped in a dark-line 2D MOT [20] which can be operated as a local quantum processor, a quantum memory, a repeater node, or an atom-photon entanglement source.

As shown in Fig. 1, to generate atom-photon entanglement, a pump pulse (Ω_p) is used to excite an atomic spin wave and generate a correlated Stokes photon (ω_s). We select two collective spin wave spatial momentum modes (+ and -), which are associated with photonic modes emitted along two distinct

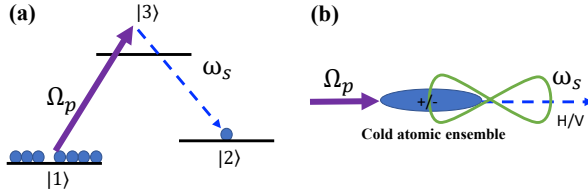


Fig. 1. Atom-Photon Entanglement (a) Energy level diagram (b) Simplified schematics for creating atom-photon entanglement

directions. Undergoing a series of optical processes, the two-photon modes ultimately result in linearly polarized H and V modes that are combined in one direction. This eventually generates an entangled state where atomic spin wave momenta (+/-) are entangled with the photonic polarizations (H/V), and this state in one atomic node can be written as:

$$(|H\rangle_s|+\rangle_a + e^{i\phi}|V\rangle_s|-\rangle_a)/\sqrt{2} \quad (1)$$

Here ϕ denotes a relative phase and can be tuned by adding an additional tunable phase retarder to one of the photonic modes.

1) Atom-Photon Entanglement with Multiple Photon Errors: Apart from the appearance of a vacuum state in spontaneous emission, the multiphoton error cannot be neglected due to the large number of atoms in an ensemble. To mitigate these errors, real experiments often employ short, low-intensity pulses to limit the single-photon emission probability to a magnitude of around 0.01. Although SeQUENCe has simulated the multiphoton error for number state entanglement, the multiphoton error in entanglement with atomic spatial modes and photonic polarization has not been simulated before.

Similar to the SPDC source used by SeQUENCe, the atom-photon entangled state generation with a cold atomic ensemble can also be modeled as a two-mode squeezed vacuum state. Using μ to denote the mean photon number, the quantum state of atom-photon entanglement encoded with spatial modes and polarizations can be written as:

$$\begin{aligned} |\phi\rangle = & a_0|0\rangle_a|0\rangle_s \\ & + a_1[\frac{1}{\sqrt{2}}(|1+\rangle_a|1H\rangle_s + |1-\rangle_a|1V\rangle_s)] \\ & + a_2[\frac{1}{\sqrt{6}}(|2+\rangle_a|2H\rangle_s + |2-\rangle_a|2V\rangle_s \\ & + 2|1-,1+\rangle_a|1H,1V\rangle_s)] \end{aligned} \quad (2)$$

where $a_0 = \frac{1}{\sqrt{\mu+1}}$ denotes the coefficient of vacuum state, $a_1 = \frac{\sqrt{\mu}}{\mu+1}$ means the coefficient of desired single photon state, and $a_2 = \sqrt{1 - \frac{1}{\mu+1} - \frac{\mu}{(\mu+1)^2}}$ is the coefficient of two photon error state. Here we have neglected the terms with more than two photons.

Enlightened by the operator ordering techniques [21], we model the atom-photon entanglement state by applying the creation operator on the vacuum state, which provides increased flexibility in the implementation of simulations. Since different

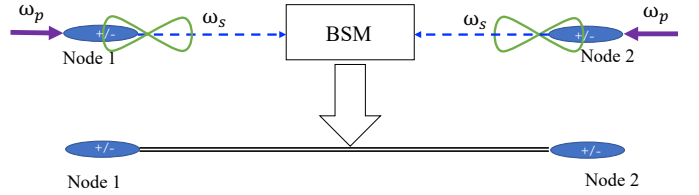


Fig. 2. Atom-Atom Entanglement

spatial modes can have different atom numbers, the atom state can be written as the tensor product of the number state in these two spatial modes $|a\rangle = |n_+\rangle \otimes |n_-\rangle$, indicating the atom numbers in $|+\rangle$ and $|-\rangle$ state are n_+ and n_- respectively. Now the basis for $|n_+\rangle$ or $|n_-\rangle$ is $(1 \ 0 \ 0)^T$, $(0 \ 1 \ 0)^T$ and $(0 \ 0 \ 1)^T$, which correspondingly represent atom number is 0, 1 and 2. Similarly, for photons, we have $|s\rangle = |n_H\rangle \otimes |n_V\rangle$ and $|n_H\rangle$ or $|n_V\rangle$ means the photon number in $|H\rangle$ or $|V\rangle$ state. Now the initial atom-photon vacuum state can be written as:

$$\begin{aligned} |\phi_1\rangle = & |0\rangle = |0_+0_-0_H0_V\rangle \\ = & |n_+=0\rangle \otimes |n_-=0\rangle \otimes |n_H=0\rangle \otimes |n_V=0\rangle \\ \equiv & \begin{pmatrix} 1 \\ 0 \\ 0 \end{pmatrix} \otimes \begin{pmatrix} 1 \\ 0 \\ 0 \end{pmatrix} \otimes \begin{pmatrix} 1 \\ 0 \\ 0 \end{pmatrix} \otimes \begin{pmatrix} 1 \\ 0 \\ 0 \end{pmatrix} \end{aligned} \quad (3)$$

We define the atomic creation operator a_+^\dagger (a_-^\dagger) to make the number of atoms in $|+\rangle$ ($|-\rangle$) increase by 1 and similarly a photonic creation operator s_H^\dagger (s_V^\dagger), where the matrix corresponding to the creation operators is

$$M_c = \begin{pmatrix} 0 & 0 & 0 \\ 1 & 0 & 0 \\ 0 & 1 & 0 \end{pmatrix} \quad (4)$$

Therefore, after using pump pulse (Ω_p) to excite atoms, the atom-photon entanglement state can be expressed with the creation operator as:

$$\begin{aligned} |\phi_1\rangle = & [a_0 + \frac{a_1}{\sqrt{2}}(a_+^\dagger s_H^\dagger + a_-^\dagger s_V^\dagger) + \frac{a_2}{\sqrt{6}}(a_+^\dagger s_H^\dagger + a_-^\dagger s_V^\dagger \\ & + 2a_+^\dagger a_-^\dagger s_H^\dagger s_V^\dagger)]|0\rangle \end{aligned} \quad (5)$$

B. Atom-Atom Entanglement

Unlike the original DLCZ protocol encoded with number states, the Bell-State Measurement(BSM) needs two-fold clicks. The joint BSM helps reduce loss due to the vacuum components and the rapid growth of multiphoton error [22]. As such, unlike SeQUENCe, there is no need to implement BSM multiple times for node-node entanglement.

1) Bell State Measurement: The joint BSM setup is depicted in Fig.3, with prepared atom-photon entanglement at Node1 and Node2. Combing a wavelength plate (HWP) and polarizing beam splitter (PBS) (HWP1 and PBS2 or HWP2 and PBS3) as a 45-degree linear polarization basis measurement, PBS1 mixes photons from different nodes, thus ideally projecting the atoms into Bell State after two-fold clicks.

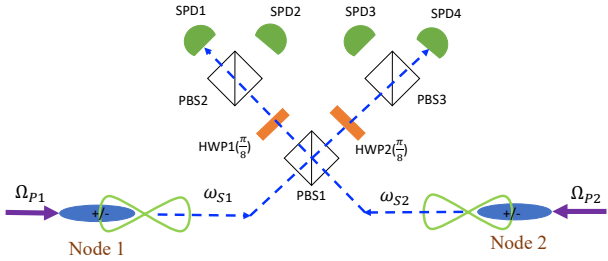


Fig. 3. BSM Node Setup

More specifically, if we have one click at SPD1, from which we can determine the photon transmitted from PBS2 and thus state before HWP1 is in state $\frac{|H\rangle+|V\rangle}{\sqrt{2}}$, where $|H\rangle$ transmits from PBS1, i.e. comes from node 2, and $|V\rangle$ reflects from PBS1, i.e. comes from node 1. In this way, the click of SPD1 indicates the photon is in state $|P_1\rangle = \frac{|V\rangle_{s1}+|H\rangle_{s2}}{\sqrt{2}}$. Similarly, the click of SPD4 measured photon as $|P_4\rangle = \frac{|H\rangle_{s1}+|V\rangle_{s2}}{\sqrt{2}}$. With two fold click of SPD1 and SPD4, we measured photons from the two nodes as $|P_{14}\rangle = \frac{1}{\sqrt{2}}(|H\rangle_{s1}|H\rangle_{s2} + |V\rangle_{s1}|V\rangle_{s2}) = |\Phi^+\rangle_{s1,s2}$.

With ideal Bell states $|\phi_{1(2)}\rangle = \frac{1}{\sqrt{2}}(|+H\rangle + |-V\rangle) = |\Phi^+\rangle_{a1,a2}$ in two nodes, we can write the two node state before BSM as

$$\begin{aligned} |\phi_{12}\rangle &= |\Phi^+\rangle_{a1,s1} \otimes |\Phi^+\rangle_{a2,s2} \\ &= \frac{1}{2}(|\Phi^+\rangle_{a1,a2}|\Phi^+\rangle_{s1,s2} + |\Phi^-\rangle_{a1,a2}|\Phi^-\rangle_{s1,s2} \\ &\quad + |\Psi^+\rangle_{a1,a2}|\Psi^+\rangle_{s1,s2} + |\Psi^-\rangle_{a1,a2}|\Psi^-\rangle_{s1,s2}) \end{aligned} \quad (6)$$

of which the density matrix can be written as $\rho_{12} = |\phi_{12}\rangle\langle\phi_{12}|$. Considering BSM as projection operator $\hat{P}_{14} = |P_{14}\rangle\langle P_{14}|$, we can get the projected atom state density matrix $\rho_a = Tr_s(\hat{P}_{14}\rho_{12}) = |\Phi^+\rangle\langle\Phi^+|_{a1,a2}$, which is obviously still a Bell state.

With this setup and we can summarize the final state of atoms with different clicks of detectors in Table.1. Noticeably,

Clicked SPDs	Measured Two-Photon State	Projected Two-Atom State
1 & 4, 2 & 3	$ \Phi^+\rangle$	$ \Phi^+\rangle$
1 & 3, 2 & 4	$ \Phi^-\rangle$	$ \Phi^-\rangle$
1 & 2, 3 & 4	NaN	NaN

TABLE I

RELATION BETWEEN CLICKED SPDs, MEASURED TWO-PHOTON STATES, AND PROJECTED TWO-ATOM STATES.

we can only distinguish two Bell states $|\Phi^\pm\rangle = \frac{1}{\sqrt{2}}(|++\rangle \pm |--\rangle)$ with the setup in Fig.3. Adding another HWP as a NOT gate enables us to detect the other two Bell states $|\Psi^\pm\rangle = \frac{1}{\sqrt{2}}(|+-\rangle \pm |-+\rangle)$, however, the maximum success rate for the most common design of polarization BSM is 50% for a specific set up due to the limitation of linear optics [23]. While there is current research aimed at pushing the limit of efficiency, in our simulator, we opt for simplicity and use the BSM design described above.

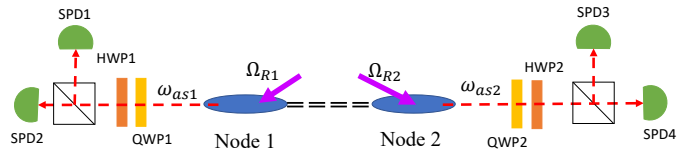


Fig. 4. Tomography

2) *BSM with Multiphoton Error Using Annihilation Operators:* Similarly to our previous definition of creation operators to generate atom-photon entanglement, we can define the detection of photons with SPD as an annihilation operator. The annihilation operators acting on photons will result in photon number decreasing 1, so we can define the annihilation operator of photons s_H and s_V similar to eq.3 as

$$M_a = \begin{pmatrix} 0 & 1 & 0 \\ 0 & 0 & 1 \\ 0 & 0 & 0 \end{pmatrix} \quad (7)$$

and have $s_H|n_H\rangle = |n_H - 1\rangle$, $s_V|n_V\rangle = |n_V - 1\rangle$.

Instead of expressing as a projection operator with state outer product, the two-fold click of SPD1 and SPD4 now can be written with annihilation operator:

$$\begin{aligned} \hat{P}_{14} &= \frac{\hat{s}_{V_1} + \hat{s}_{H_2}}{\sqrt{2}} \otimes \frac{\hat{s}_{H_1} + \hat{s}_{V_2}}{\sqrt{2}} \\ &= \frac{1}{2}(\hat{s}_{H_1}\hat{s}_{V_1} + \hat{s}_{H_1}\hat{s}_{H_2} + \hat{s}_{V_1}\hat{s}_{V_2} + \hat{s}_{H_2}\hat{s}_{V_2}) \\ &= \frac{1}{2}(\hat{s}_{H_1} \otimes \hat{s}_{V_1} \otimes I_{H_2} \otimes I_{V_2} + \hat{s}_{H_1} \otimes I_{V_1} \otimes \hat{s}_{H_2} \otimes I_{V_2} \\ &\quad + I_{H_1} \otimes \hat{s}_{V_1} \otimes I_{H_2} \otimes \hat{s}_{V_2} + I_{H_1} \otimes I_{V_1} \otimes \hat{s}_{H_2} \otimes \hat{s}_{V_2}) \end{aligned} \quad (8)$$

Since the photon detectors are not able to resolve the photon number, the clicks of SPDs is equivalent to taking a trace of all photon number states. So the final state of atom1 and atom2 after SPD1 and SPD4 click as follows:

$$\rho_{a1,a2} = \sum_{i,j,k,l} \langle i,j,k,l | \hat{P}_{14} \rho_{12} \hat{P}_{14}^\dagger | i,j,k,l \rangle \quad (9)$$

where

$$\begin{aligned} |i,j,k,l\rangle &= I_{+1} \otimes I_{-1} \otimes s_{H_1}^{\dagger i} \begin{pmatrix} 1 \\ 0 \\ 0 \end{pmatrix} \otimes s_{V_1}^{\dagger j} \begin{pmatrix} 1 \\ 0 \\ 0 \end{pmatrix} \\ &\quad \otimes I_{+2} \otimes I_{-2} \otimes s_{H_2}^{\dagger k} \begin{pmatrix} 1 \\ 0 \\ 0 \end{pmatrix} \otimes s_{V_2}^{\dagger l} \begin{pmatrix} 1 \\ 0 \\ 0 \end{pmatrix} \end{aligned} \quad (10)$$

Therefore, we can get the corresponding state of atoms after either two of the four detectors click and their corresponding probability by

$$P_{\text{succ}} = \text{Tr}(\rho_{a1,a2}) \quad (11)$$

C. Quantum Tomography of Atoms

To evaluate the fidelity of the entangled atomic state, we apply a read pulse to convert the atomic states into photon states followed by coincident measurement to perform tomography of photon states, as shown in Fig.4. Since the coincident

measurement of photons from two nodes naturally eliminates the states containing vacuum state in either node, the two-photon noise states $|2H(V)\rangle_{as1}|0\rangle_{as2}$, $|1H1V\rangle_{as1}|0\rangle_{as2}$, $|0\rangle_{as1}|2H(V)\rangle_{as2}$ and $|0\rangle_{as1}|1H1V\rangle_{as2}$ will not contribute to the infidelity. Furthermore, using a different basis set up for the next step of entanglement swapping, these two-photon noise states will not cause successful events. Therefore, compared to DLCZ protocol with number state, the spurious growth of multiphoton errors is restrained in this protocol. We eliminated the two-photon noise states mentioned above and get an effective density matrix $\hat{\rho}_{a_1, a_2 \text{ eff}}$. Then the effective fidelity of the entangled atom state can be evaluated as

$$\tilde{F} = \frac{\text{Tr}(\langle \Phi^+ | \hat{\rho}_{a_1, a_2 \text{ eff}} | \Phi^+ \rangle)}{\text{Tr}(\hat{P}_F \hat{\rho}_{a_1, a_2 \text{ eff}} \hat{P}_F^\dagger)}. \quad (12)$$

Since only two-atom states will contribute to the fidelity, it is easier to extract two-atom states (4 by 4 density matrix) from the enlarged computation space with multi-atom and vacuum states (81 by 81 density matrix) before modeling the tomography process. With enlarged computation space, the basis of atom states of two nodes can be written as

$$|b_{12}\rangle = |n_{+1}, n_{-1}, n_{+2}, n_{-2}\rangle \quad (13)$$

With this definition, the two-atom states correspond to $|n_{+1} = 1, n_{-1} = 0, n_{+2} = 1, n_{-2} = 0\rangle$, $|n_{+1} = 1, n_{-1} = 0, n_{+2} = 0, n_{-2} = 1\rangle$, $|n_{+1} = 0, n_{-1} = 1, n_{+2} = 1, n_{-2} = 0\rangle$ or $|n_{+1} = 0, n_{-1} = 1, n_{+2} = 0, n_{-2} = 1\rangle$, and thus we can determine the position of a non-zero element by $n_{+1} \times 3^3 + n_{-1} \times 3^2 + n_{+2} \times 3^1 + n_{-2} \times 3^0$. Then we enumerate all of these possibilities to get the entry from 81 by 81 matrix and construct the 4 by 4 matrix as we need.

We used a similar methodology in [24] to perform exact tomography on two photons, where the state can be represented by

$$\rho_{1,2} = \frac{1}{4} \sum_{k_1, k_2} a_{k_1, k_2} \hat{\sigma}_{k_1} \hat{\sigma}_{k_2} (k_1, k_2 = 0, 1, 2, 3) \quad (14)$$

Let $\hat{\sigma}_{k_i}$ represent the k -th Pauli operator acting on the i -th photon. To reconstruct the original density matrix, we need to compute the 15 Stokes parameters a_{k_i} in Eq.14 (with normalization requiring $a_{00} = 1$). We set up nine experimental configurations, each with four measurements, resulting in a total of 36 measurement outcomes. Using these results, we calculate the respective Stokes parameters and subsequently reconstruct the density matrix.

IV. SIMULATOR DESIGN

In this section, we provide a brief overview of the proposed simulator. We first introduce the key concepts and design logic of the SeQUENCe simulator. Then we discuss how we integrated the models in A²Tango and highlight the differences between the two simulators. Our main contributions include the Atomic Node and the BSM models .

A. SeQUENCe Overview

SeQUENCe is a modular, discrete-event quantum network simulator designed to simulate physical hardware and network behavior in quantum networks. Its main architecture comprises five modules, namely: the Simulator Kernel, a.k.a. the simulation engine, hardware, Entanglement Manager, Resource Manager, Network Manager, and Applications. The Hardware Manager module models and simulates key physical components, such as quantum channels, photons, quantum memory, and experimental devices. The Entanglement Manager encompasses various protocol models for entanglement generation, purification, and swapping, serving as the "software" running on physical devices. The Resource Manager module supervises local resources in a quantum network by allocating hardware resources, tracking memory states, and coordinating entanglement protocol instances. Network Management enables applications to reserve network resources, while Applications define entanglement consumption. The Kernel, another vital component, consists of a discrete event simulator and a quantum manager that handle time advancement and quantum state management, respectively. Our work primarily extends SeQUENCe's Hardware module .

B. Atomic Node

The atomic ensemble is a crucial component in our simulator, functioning similarly to the 'memory' class in the SeQUENCe simulator. In our approach, the atomic ensemble is utilized to generate atom-photon and atom-atom entanglement, as well as to operate as quantum memory for reading and writing incoming photon states. It is important to note that our work employs quantum memory to store and retrieve flying photonic quantum states, akin to recent experimental progress as reported in [25]. Our abstraction for the atomic ensemble uses the 'AtomicNode' class, which inherits from SeQUENCe's Entity class. AtomicNode primarily has the following functions: atomPhoton_single_entangle, atomPhoton_multiple_entangle, write, and read. The atomPhoton_single_entangle function models the process where atomic ensembles generate atom-photon entanglement without spontaneous emission errors, while atomPhoton_multiple_entangle models the spontaneous emission errors themselves. The write and read methods model the process that the atomic node uses as quantum memory to retrieve and store photon state which will be later used to generate longer multi-hop entanglements. To model quantum memory performance, we use an efficiency table to describe how the decoherence over time of state stored in quantum memory.

C. Bell State Measurement

The original SeQUENCe design features a BSM class, which encompasses a 'Polarization BSM' that models a polarization BSM device. This device can measure incoming photons based on polarization and manage entanglement. However, it doesn't align with the Bell State Measurement model previously outlined in Section III. Our

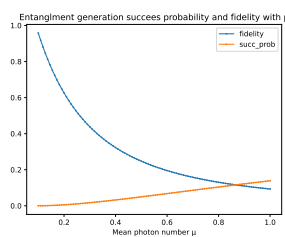


Fig. 5. Success Probability and Fidelity of Entanglement as a function of the mean photon number

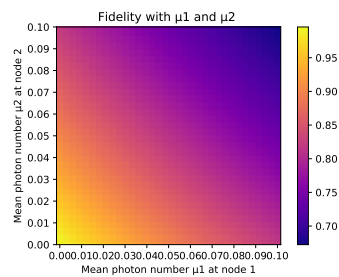


Fig. 6. Fidelity of generated entanglement as a function of the mean photon number of two atomic ensembles

design is analogous to how we model atom-photon entanglement with and without spontaneous emission error. We created classes `PolarizationSingleBSM` and a `PolarizationMultipleBSM`, both of which inherit from `SeQUENCe's BSM class`. The general process of how these two BSMs work is as follows. When photons are retrieved from both sides of two remote quantum nodes, the BSM class calls the 'get' method, signaling the BSM to perform a Bell State Measurement. This process first models different detectors' click operators and uses them to act on the incoming photon state. By calculating the trace of the post-detection state, we can simulate the probability distribution of the clicks of two out of the four detectors. The key distinction between the two BSMs is that the `PolarizationSingleBSM` uses a positive operator-valued measure (POVM), while the `PolarizationMultipleBSM` employs annihilation operators and their corresponding spaces to model Bell State Measurement, which includes detecting multiple photons.

V. SIMULATION RESULTS

A. Effective Entangled Fidelity and Success Probability

In this section, we show some preliminary results obtained using our simulator, namely the direct success probability and calculated fidelity of generated atom-atom entangled state. Both metrics are important to study the performance of atom-atom entanglement generation and provide insights for experiments with parameter optimization.

In real quantum network process, as long as there are expected two-fold clicks in BSM, we consider the event successful and continue the next step of entanglement swapping. Apparently, we cannot eliminate the multi-atom false state with only the information of two-fold clicks, which can be demonstrated by the imperfect effective fidelity.

In order to calculate entanglement fidelity, we take states where either node is a vacuum state as loss as discussed in Section III.C. After introducing the loss by setting corresponding elements in the density matrix as zero, we renormalize the density matrix and calculate the effective fidelity with measurement by expected Bell State.

As shown in Fig. 5, a higher mean photon number will have a higher success probability, which can be understood as less loss. However, increasing the mean photon number causes a decrease in the effective fidelity, because the amplitude of

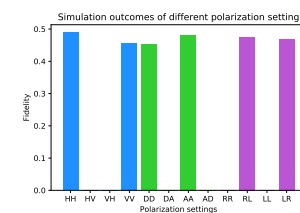


Fig. 7. Simulation outcomes of the Fig. 8. Reconstructed density matrix fractions at different polarization settings

multiphoton error also grows. Therefore, with a given pump pulse excitation rate, one can figure out the optimized mean photon number to approach both reasonable entanglement generation rate and effective fidelity.

B. Density Matrix Reconstruction

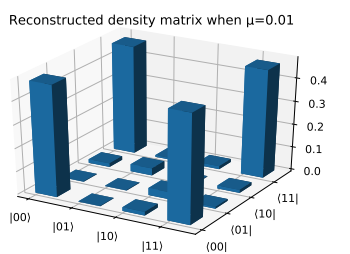
In this section, we characterize the generated atom-atom entanglement by simulating the two-photon tomography as discussed in Section III.C. As an example, we take the condition in demonstrated experiment [7], in which the excitation probability is 0.01, giving the mean photon number around 0.01. We conduct 9×1000 measurements to obtain probabilities of 36 components as required in [24]. In Fig. 6, we show how the fidelity of entanglement varies with two different mean photon numbers at two atomic ensembles, we can see a clear symmetric relation of two nodes. In Fig. 7, we show the measured probabilities of components contained in the expected Bell State. After obtaining the 36 probabilities, we reconstruct the density matrix in two-photon space as shown in Fig. 8. We notice that the reconstructed density matrix is almost the same as Bell State $|\Phi^+\rangle$ as expected since we have not introduced other decoherence. The trace of the density matrix is not one due to the multiphoton error being excluded from the two-photon space, thus we can get the effective fidelity as the trace here.

VI. CONCLUSION

In this work, we develop a simulator for entanglement generation between two remote atomic ensembles, called A²Tango, by extending the SeQUENCe open-source quantum network simulator. A²Tango models the atomic ensembles and demonstrates how basic quantum operations including atom-photon entanglement and atom-atom entanglement, Bell State Measurement, and quantum tomography can be realized. Specifically, A²Tango models multi-photon events during the local excitation and propagation and includes such errors in simulations. We show the relation of entanglement generation rate and fidelity as a function of mean photon number and A²Tango reconstructs the state using the quantum tomography introduced.

ACKNOWLEDGMENT

The authors were partially supported by NSF Grants 1750704, 2114076, 1932447, and 2114113, DoE Grant DE-SC0022069, and AFOSR Grant FA9550-22-1-0043. We thank the anonymous reviewers for their comments.



REFERENCES

- [1] H.-J. Briegel, W. Dür, J. I. Cirac, and P. Zoller, “Quantum repeaters: The role of imperfect local operations in quantum communication,” *Phys. Rev. Lett.*, vol. 81, pp. 5932–5935, Dec 1998. [Online]. Available: <https://link.aps.org/doi/10.1103/PhysRevLett.81.5932>
- [2] S.-H. Wei, B. Jing, X.-Y. Zhang, J.-Y. Liao, C.-Z. Yuan, B.-Y. Fan, C. Lyu, D.-L. Zhou, Y. Wang, G.-W. Deng *et al.*, “Towards real-world quantum networks: a review,” *Laser & Photonics Reviews*, vol. 16, no. 3, p. 2100219, 2022.
- [3] Y. Wang, J. Li, S. Zhang, K. Su, Y. Zhou, K. Liao, S. Du, H. Yan, and S.-L. Zhu, “Efficient quantum memory for single-photon polarization qubits,” *Nat. Photon.*, vol. 13, pp. 346–351, May 2019. [Online]. Available: <https://doi.org/10.1038/s41566-019-0368-8>
- [4] E. Oh, X. Lai, J. Wen, and S. Du, “Distributed quantum computing with photons and atomic memories,” *Advanced Quantum Technologies*, vol. n/a, no. n/a, p. 2300007. [Online]. Available: <https://onlinelibrary.wiley.com/doi/abs/10.1002/qute.202300007>
- [5] Z.-B. Chen, B. Zhao, Y.-A. Chen, J. Schmiedmayer, and J.-W. Pan, “Fault-tolerant quantum repeater with atomic ensembles and linear optics,” *Physical Review A*, vol. 76, no. 2, p. 022329, 2007.
- [6] B. Zhao, Z.-B. Chen, Y.-A. Chen, J. Schmiedmayer, and J.-W. Pan, “Robust creation of entanglement between remote memory qubits,” *Physical review letters*, vol. 98, no. 24, p. 240502, 2007.
- [7] Z.-S. Yuan, Y.-A. Chen, B. Zhao, S. Chen, J. Schmiedmayer, and J.-W. Pan, “Experimental demonstration of a bdcz quantum repeater node,” *Nature*, vol. 454, no. 7208, pp. 1098–1101, 2008.
- [8] L.-M. Duan, M. D. Lukin, J. I. Cirac, and P. Zoller, “Long-distance quantum communication with atomic ensembles and linear optics,” *Nature*, vol. 414, no. 6862, pp. 413–418, 2001.
- [9] H.-J. Briegel, W. Dür, J. I. Cirac, and P. Zoller, “Quantum repeaters: the role of imperfect local operations in quantum communication,” *Physical Review Letters*, vol. 81, no. 26, p. 5932, 1998.
- [10] D. L. Moehring, P. Maunz, S. Olmschenk, K. C. Younge, D. N. Matsukevich, L.-M. Duan, and C. Monroe, “Entanglement of single-atom quantum bits at a distance,” *Nature*, vol. 449, no. 7158, pp. 68–71, 2007.
- [11] T. Wilk, S. C. Webster, A. Kuhn, and G. Rempe, “Single-atom single-photon quantum interface,” *Science*, vol. 317, no. 5837, pp. 488–490, 2007.
- [12] Y.-A. Chen, S. Chen, Z.-S. Yuan, B. Zhao, C.-S. Chuu, J. Schmiedmayer, and J.-W. Pan, “Memory-built-in quantum teleportation with photonic and atomic qubits,” *Nature Physics*, vol. 4, no. 2, pp. 103–107, 2008.
- [13] S.-J. Yang, X.-J. Wang, X.-H. Bao, and J.-W. Pan, “An efficient quantum light-matter interface with sub-second lifetime,” *Nature Photonics*, vol. 10, no. 6, pp. 381–384, 2016.
- [14] X. Wu, A. Kolar, J. Chung, D. Jin, T. Zhong, R. Kettimuthu, and M. Suchara, “Sequence: a customizable discrete-event simulator of quantum networks,” *Quantum Science and Technology*, vol. 6, no. 4, p. 045027, 2021.
- [15] T. Coopmans, R. Knegjens, A. Dahlberg, D. Maier, L. Nijsten, J. de Oliveira Filho, M. Papendrecht, J. Rabbie, F. Rozpedek, M. Skrzypczyk *et al.*, “Netsquid, a network simulator for quantum information using discrete events,” *Communications Physics*, vol. 4, no. 1, p. 164, 2021.
- [16] A. Dahlberg and S. Wehner, “Simulaqron—a simulator for developing quantum internet software,” *Quantum Science and Technology*, vol. 4, no. 1, p. 015001, 2018.
- [17] S. DiAdamo, J. Nötzel, B. Zanger, and M. M. Beše, “Qunetsim: A software framework for quantum networks,” *IEEE Transactions on Quantum Engineering*, vol. 2, pp. 1–12, 2021.
- [18] B. Bartlett, “A distributed simulation framework for quantum networks and channels,” *arXiv preprint arXiv:1808.07047*, 2018.
- [19] R. Satoh, M. Hajdušek, N. Benchasattabuse, S. Nagayama, K. Teramoto, T. Matsuo, S. A. Metwalli, P. Pathumsoot, T. Satoh, S. Suzuki *et al.*, “Quisp: a quantum internet simulation package,” in *2022 IEEE International Conference on Quantum Computing and Engineering (QCE)*. IEEE, 2022, pp. 353–364.
- [20] S. Zhang, J. F. Chen, C. Liu, S. Zhou, M. M. T. Loy, G. K. L. Wong, and S. Du, “A dark-line two-dimensional magneto-optical trap of 85rb atoms with high optical depth,” *Rev. Sci. Instrum.*, vol. 83, no. 7, p. 073102, 2012. [Online]. Available: <https://doi.org/10.1063/1.4732818>
- [21] M. J. Collett, “Exact density-matrix calculations for simple open systems,” *Phys. Rev. A*, vol. 38, pp. 2233–2247, Sep 1988. [Online]. Available: <https://link.aps.org/doi/10.1103/PhysRevA.38.2233>
- [22] L. Jiang, J. M. Taylor, and M. D. Lukin, “Fast and robust approach to long-distance quantum communication with atomic ensembles,” *Phys. Rev. A*, vol. 76, p. 012301, Jul 2007. [Online]. Available: <https://link.aps.org/doi/10.1103/PhysRevA.76.012301>
- [23] N. Lütkenhaus, J. Calsamiglia, and K.-A. Suominen, “Bell measurements for teleportation,” *Phys. Rev. A*, vol. 59, pp. 3295–3300, May 1999. [Online]. Available: <https://link.aps.org/doi/10.1103/PhysRevA.59.3295>
- [24] J. B. Altepeter, D. F. James, and P. G. Kwiat, “4 qubit quantum state tomography,” *Quantum state estimation*, pp. 113–145, 2004.
- [25] Y. Wang, J. Li, S. Zhang, K. Su, Y. Zhou, K. Liao, S. Du, H. Yan, and S.-L. Zhu, “Efficient quantum memory for single-photon polarization qubits,” *Nature Photonics*, vol. 13, no. 5, pp. 346–351, 2019.